Hindawi Publishing Corporation
International Journal of Antennas and Propagation
Volume 2012, Article ID 150267, 10 pages
doi:10.1155/2012/150267

Research Article

Statistical Modeling of Ultrawideband Body-Centric Wireless Channels Considering Room Volume

Miyuki Hirose, Hironobu Yamamoto, and Takehiko Kobayashi

Wireless Systems Laboratory, Tokyo Denki University, 5 Senju-Asahi-Cho, Adachi-Ku, Tokyo 120-8551, Japan

Correspondence should be addressed to Miyuki Hirose, miyuki@grace.c.dendai.ac.jp

Received 31 July 2012; Accepted 12 October 2012

Academic Editor: César Briso Rodríguez

Copyright © 2012 Miyuki Hirose et al. This is an open access article distributed under the Creative Commons Attribution License, which permits unrestricted use, distribution, and reproduction in any medium, provided the original work is properly cited.

This paper presents the results of a statistical modeling of onbody ultrawideband (UWB) radio channels for wireless body area network (WBAN) applications. Measurements were conducted in five different rooms. A measured delay profile can be divided into two domains; in the first domain ($0 < t \leq 4$ ns) there is either a direct (for line of sight) or diffracted (for nonline of sight) wave which is dependent on the propagation distance along the perimeter of the body, but essentially unrelated to room volume, and the second domain ($t > 4$ ns) has multipath components that are dominant and dependent on room volume. The first domain was modeled with a conventional power decay law model, and the second domain with a modified Saleh-Valenzuela model considering the room volume. Realizations of the impulse responses are presented based on the composite model and compared with the measured average power delay profiles.

1. Introduction

Wireless onbody area communication technologies are significant for both medical and nonmedical applications. Ultrawideband (UWB) technologies have been considered for use in wireless body area networks (WBANs) because of their possible low power consumption and antimultipath capabilities. Numerous studies have been carried out on UWB propagation characterization and the modeling of indoor UWB communication channels. A number of measurements relating to WBAN have been carried out to characterize and model on- and offbody UWB propagation in either a radio anechoic chamber or a specific room type [1–4]. The conventional UWB propagation loss model in these studies, however, did not consider the impact of surrounding environments. Since multipaths (in particular, the reflected waves from floors, walls, and ceilings) depend strongly on room volume, it is necessary to evaluate the variation of propagation characteristics in various environments. To address this problem, we measured UWB (3.1–10.6 GHz) radio propagation around the human body in a radio anechoic chamber and four different rooms and proposed a new UWB propagation loss model depending on the room volume [5]. In this study, time-domain statistical channel model will be the presented based on the same measurement campaign as [5].

As for statistical modeling of the channel impulse response, Fort et al. [3] separated the WBAN propagation channels into two parts: (1) diffraction around the body and (2) reflections off of nearby scatterers then back at the body, and modeled the second part using a modified Saleh-Valenzuela (SV) model [6]. The applicable area of the modified SV model in [6], however, was limited to wireless personal area networks not including human bodies. Roblin [7] scrutinized the separability of channels for various scenarios in three different rooms, concluded that UWB channels can be separated in the case of a relatively larger room, but it has not established a channel model. We also divided the channel responses into two parts which were then modeled by power decay law and a modified SV model depending on the room volume.

2. Measurement Setup

The measurement campaigns were conducted in five parallelepiped rooms as shown in Figure 1. The dimensions of Room A (a radio anechoic chamber) were measured

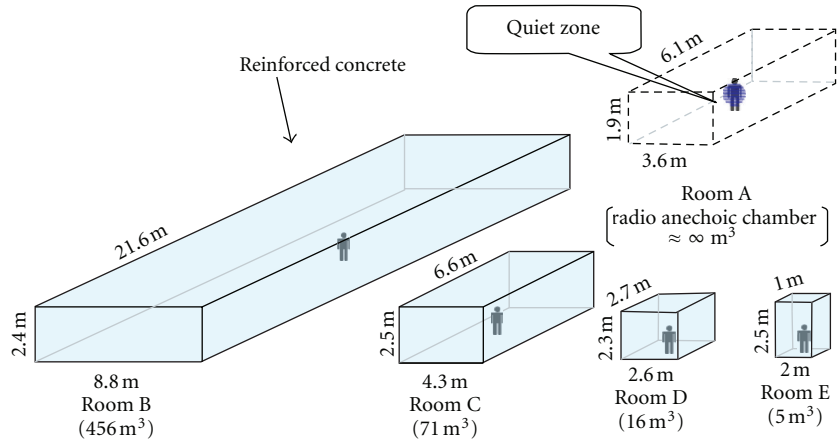

Figure 1: The outline of five rooms used for experiments.

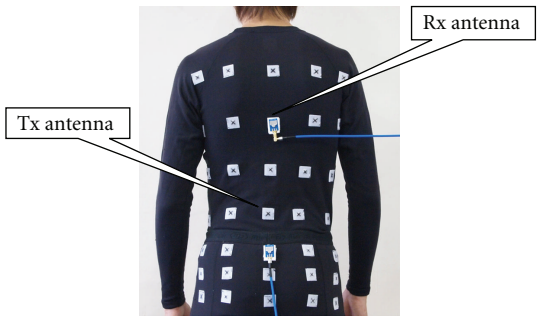

Figure 2: Placement of transmitting and receiving antennas on the body. Rectangular patches on the clothes are fabric hook-and-loop fasteners to fix the antennas.

between the apexes of the radio absorbers paneled on all surfaces. The radio anechoic chamber can be considered as a room extending to an infinite volume (i.e., free space) in terms of radio propagation. Rooms B to E were made of reinforced concrete, and their floors, walls, and ceilings were mostly covered with, respectively, linoleum, wallpaper, and plasterboard, all of which were lossy dielectrics. The measurements were carried out using a human subject (adult male, 1.72 m tall and 56 kg). The subject stood upright with the feet shoulder width apart in either a quiet zone of the radio anechoic chamber or the center of Rooms B to E. The UWB (3.1–10.6 GHz) propagation losses were measured with a vector network analyzer (VNA) between onbody meander line antennas [8]. The voltage standing wave ratio of the antennas was less than 2.5 between 3.1 and 10.6 GHz, and the omnidirectionality in the horizontal plane was within 3 dB in a free space. The transmitting antenna was fixed on the center back waist of the subject and placed at a height of 1.0 m from the floor, as shown in Figure 2. The receiving antenna was placed at approximately 100 mm intervals on the torso. Both antennas were vertically polarized and separated 10 mm from the subject body. When the receiving antenna was placed on the back of the subject's body, the path was roughly line of sight (LOS), and when on the front, it was non-LOS (NLOS). In total 69 receiving points around the torso were employed. The transmitting and receiving antennas were fed via coaxial cables, perpendicular to each other in configuration without crossing to reduce undesired cable coupling [9]. The calibration was conducted between the feeding points with a coaxial through adaptor. The frequency-domain transfer function (size = 1,024 = 751 measured within the 7.5-GHz bandwidth + 273 zero padding) was inversely Fourier transformed into a delay profile with the use of a rectangular window. Major specifications of the measurements are listed in Table 1.

Table 1: Specifications of the propagation measurements [5].

Bandwidth	3.1–10.6 GHz
Frequency sweeping points by VNA	751 points, 10-MHz interval
Calibration	Internal function of the VNA
Antennas	Meanderline UWB antennas [8]

3. Measurement Results and Modeling

Examples of the delay profiles when the receiving antenna was placed on the center chest (NLOS) and the back side (LOS) of the subject are presented in Figure 3. An increase in total received power was observed when the room volume was decreased (see Appendix A). This was attributed to the more affluent multipaths from the nearby floor, walls, and ceiling in Rooms B to E. The dominant propagation path in Room A (the radio anechoic chamber) was either a direct or a diffracted (around the body) wave, and thus the total reception power is lower than that in the other rooms. With decreasing room volume, mean free path lengths decreased, the power component contained in the multipaths increased, and consequently the total received power increased.

3.1. Division of Propagation Channels. A delay profile can be treated by dividing it into two domains, in the same way as [3, 7]: the first (approximately arriving time $0 < t \leq 4$ ns)

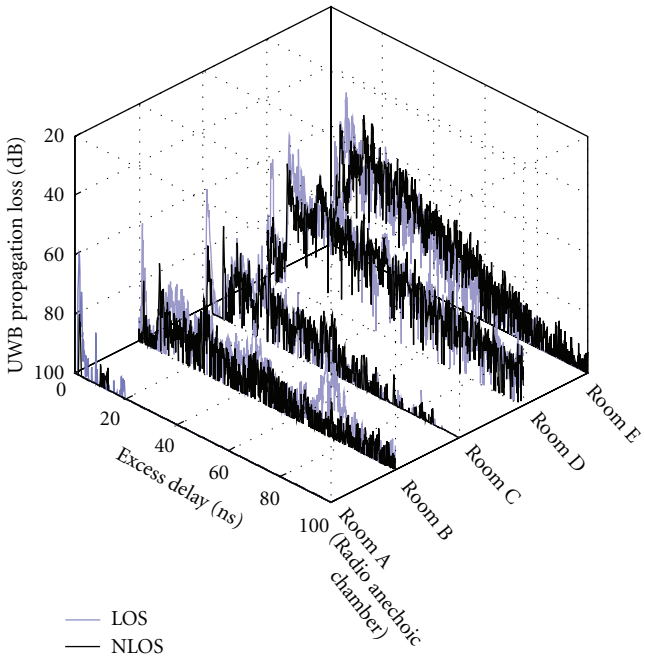

Figure 3: Example of the delay profiles measured in Rooms A to E [5].

and second ($t > 4$ ns) domains, as schematically shown in Figure 4. The first domain represents the contribution of the human alone, consisting of either direct (for LOS) or diffracted (for NLOS) wave measured in free space or radio anechoic chambers. And the second domain represents the contribution of the surrounding environments, consisting of remaining multipath components, which depend on room volume. Justification for dividing the profiles at $t = 4$ ns is given in Appendix B.

3.2. Statistical Analysis of the First Domain. The channel response in the first domain ($0 < t \leq 4$ ns) can be represented by

$$h_1(t) = h_{10} \cdot \left(\frac{d}{d_0}\right)^n \cdot \delta(t - t_0), \tag{1}$$

where h_{10} is the propagation gain at the reference distance d_0 ($= 0.1$ m), d is the propagation distance along the perimeter of the body, n is the propagation loss exponent, t_0 is the arrival time of the first wave, and $\delta(\cdot)$ is the Dirac delta function. The arrival time t_0 is proportional to d. Equation (1) represents a special case (when the room volume $V = \infty$) of the previously proposed UWB propagation loss model depending on room volume [5] (see Appendix C). The values of h_{10} and n in (1) were found to be 4.3×10^{-4} and 3.8 for LOS and 3.2×10^{-5} and 5.1 for NLOS, respectively, from the data of PL_{dB} shown in Figure 5. The statistics of the $h_1(t)$ followed lognormal distribution with a standard deviation of 4.4 dB (±0.5 dB) and 3.4 dB (±0.5 dB), for LOS and NLOS, respectively, where the values in the parentheses indicate 95% confidence intervals.

Table 2: Parameters of the first arriving multipath component.

	NLOS	LOS
ν	−2.8	−3.0
β_0	59.1	52.4

3.3. Statistical Analysis of the Second Domain. The second domain ($t > 4$ ns) can be represented by a modified SV model [6] based on a cluster concept of rays:

$$h_2(t) = \sum_{l=0}^{\infty} \sum_{k=0}^{\infty} \beta_{k,l} \delta(t - T_l - \tau_{k,l}), \tag{2}$$

where $\{\beta_{k,l}\}$ are the multipath gain coefficients, $\{T_l\}$ is the delay of the lth cluster, and $\{\tau_{k,l}\}$ is the delay of the kth multipath component relative to the lth cluster arrival time (T_l). Delay profiles measured in Rooms B, C, D, and E indicated that rays arrived in clusters, as shown in Figure 6, where the abscissas of the graphs are drawn in antilogarithm. While Fort et al. stated cluster interval times fit to the Weibull distribution [3], in all our cases, the arrival time intervals of the clusters were found to follow an exponential distribution by using Kolmogorov-Smirnov (K-S) test with a 95% confidence interval. This means that cluster arrivals are modeled as a Poisson arrival process with a fixed rate of Λ [1/ns]. Within each cluster, subsequent rays also arrived according to a Poisson process with another fixed rate of λ [1/ns]. The distribution of the cluster and ray arrival times are given by

$$\begin{aligned} p(T_l \mid T_{l-1}) &= \Lambda \exp[-\Lambda(T_l - T_{l-1})], \quad l > 0, \\ p(\tau_{k,l} \mid \tau_{(k-1),l}) &= \lambda \exp[-\lambda(\tau_{k,l} - \tau_{(k-1),l})], \quad k > 0, \end{aligned} \tag{3}$$

where Λ and λ are cluster arrival rate and ray arrival rate within each cluster, respectively. The IEEE 802.15.4a channel model [6] used a lognormal distribution rather than a Rayleigh distribution adopted in the original S-V model [10] for the multipath gain coefficients $\beta_{k,l}$. We also adopted a lognormal distribution for $\beta_{k,l}$ because of a better fitting to the measured data. The average power of both the clusters and the rays within the clusters are assumed to decay exponentially, such that the average power of the multipath component at a given delay $T_l + \tau_{k,l}$ is given by

$$\left\langle \beta_{k,l}^2 \right\rangle = \left\langle \beta_{0,0}^2 \right\rangle \exp\left(-\frac{T_l}{\Gamma}\right) \exp\left(-\frac{\tau_{k,l}}{\gamma}\right), \tag{4}$$

where $\langle \beta_{0,0}^2 \rangle$ is the expected value of the power of the first arriving multipath component, Γ is the delay exponent of the clusters, and γ is the decay exponent of the rays within a cluster. The first arriving multipath detected in measured delay profiles is lower with decreased room volume, as shown in Figure 7. The first multipath component, $\langle \beta_{0,0}^2 \rangle$, can be represented by

$$\left\langle \beta_{0,0}^2 \right\rangle = \beta_0 \cdot \left(\sqrt[3]{V}\right)^{\nu}. \tag{5}$$

The values of β_0 and ν are listed in Table 2.

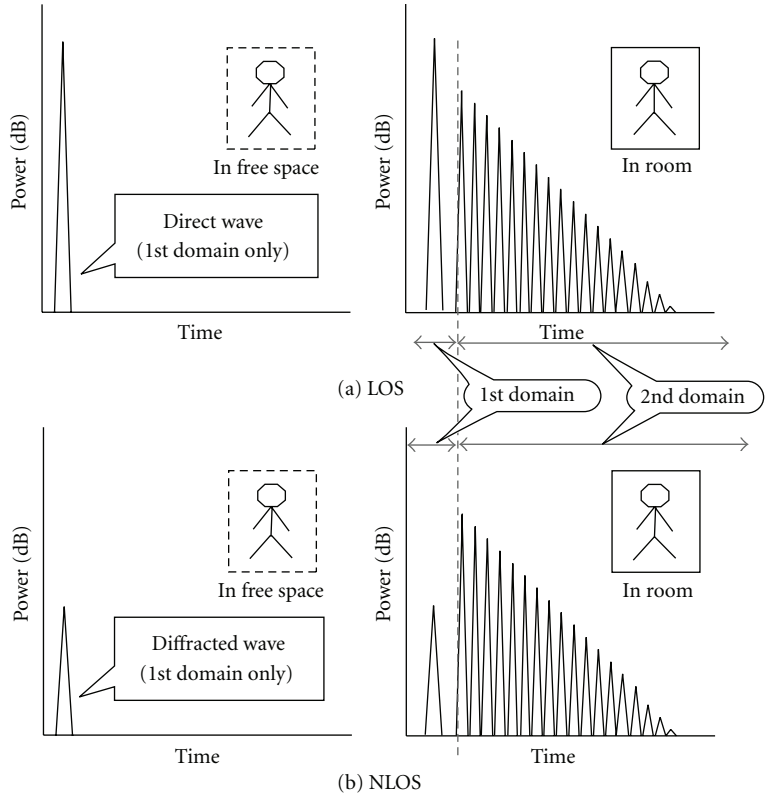

Figure 4: Conceptual diagram of the division of the delay profiles: (a) LOS and (b) NLOS. The first domain represents the delay profiles measured in free space or radio anechoic chambers and contains a direct or diffracted wave along the body. The second domain consists of the remaining multipath components.

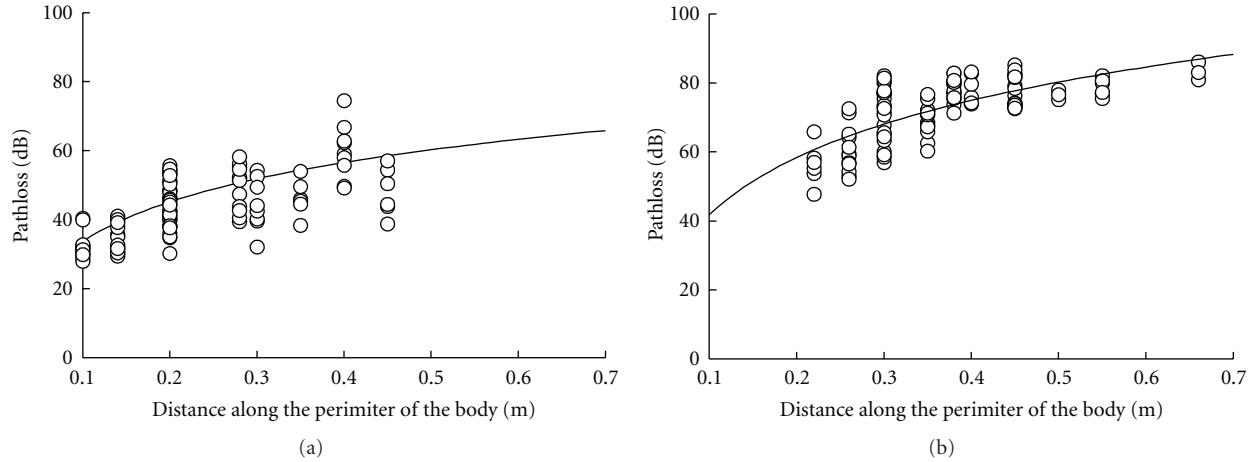

Figure 5: Ultrawideband pathloss onbody antennas measured in a radio anechoic chamber: (a) LOS and (b) NLOS.

The values of Λ, λ, Γ, and γ were derived from the delay profile data measured in Rooms B, C, D, and E. Figures 8 and 9 present those values against $V^{1/3}$ along with regression lines. Note that $V^{1/3}$ represents the mean free path length of the rays traveling within a room having a finite (or infinite) volume V. The cluster arrival time rate Λ[1/ns] is approximately 0.08, while the ray arrival time rate λ [1/ns] is 0.4 for both LOS and NLOS. While the arrival rates Λ and λ exhibited no apparent dependence on $V^{1/3}$ or LOS/NLOS scenarios as shown in Figure 8, the power decay factors Γ and γ slightly increased with $V^{1/3}$, as shown in Figure 9. The propagation distances (and therefore propagation losses) of rays increase with the room volume, and therefore the decay factors increase. The slope was steeper for the NLOS than for the LOS cases. The dependence of the cluster power-decay factor and

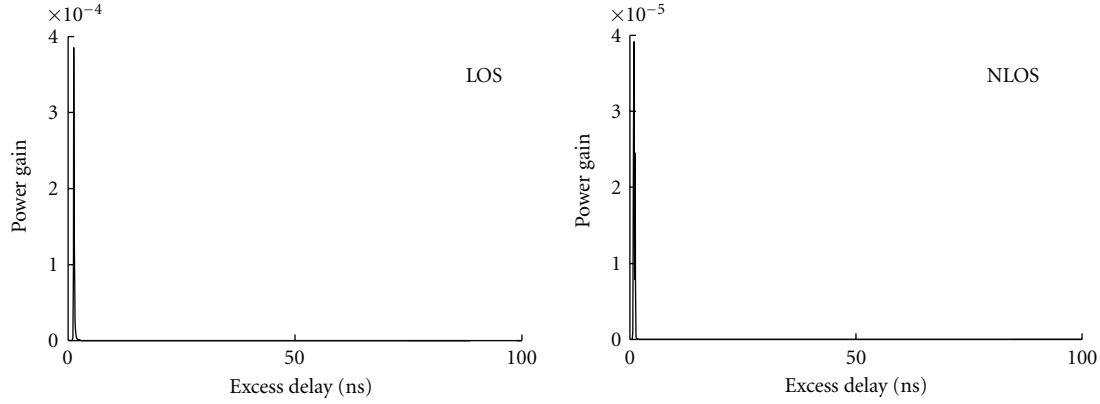

(a) Room A

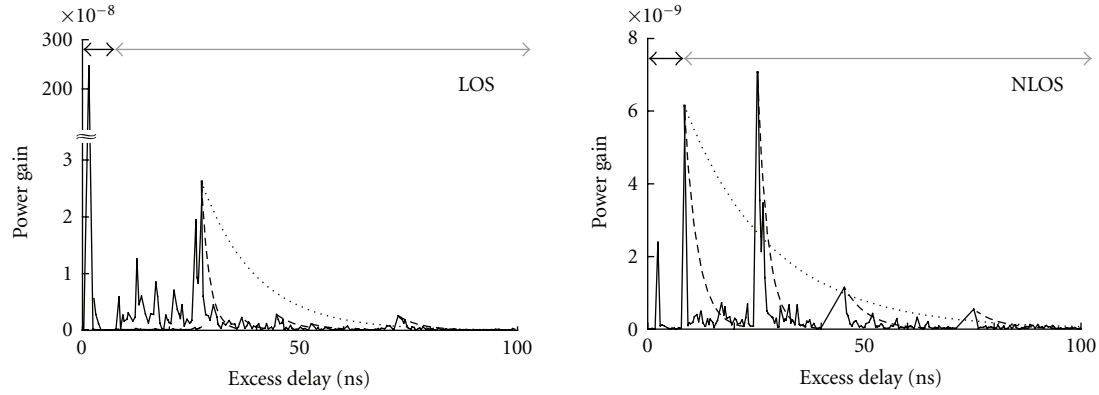

(b) Room B

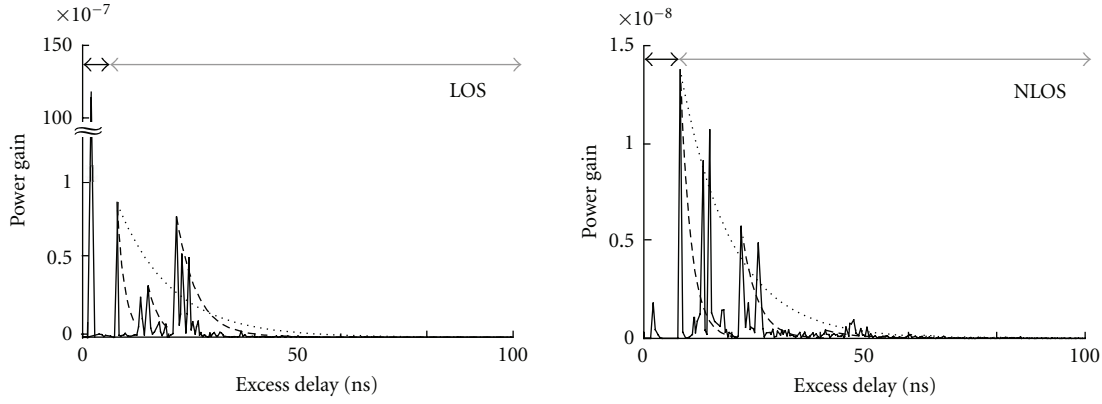

(c) Room C

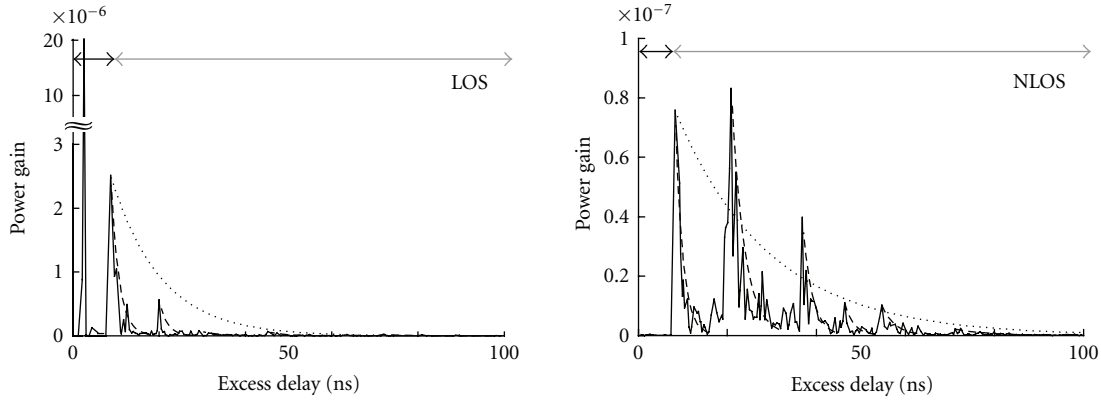

(d) Room D

Figure 6: Continued.

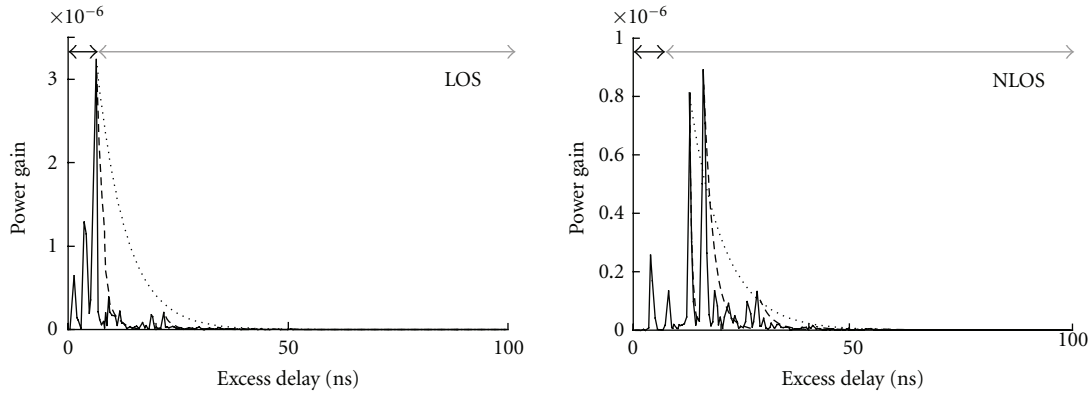

(e) Room E

Figure 6: Examples of the delay profiles measured in Rooms A to E. Profiles for LOS were measured at the center of the back and those for NLOS at the center of the chest. The dashed lines represent exponential power decay of the rays and the clusters. The black and grey arrows indicate the first and the second domains.

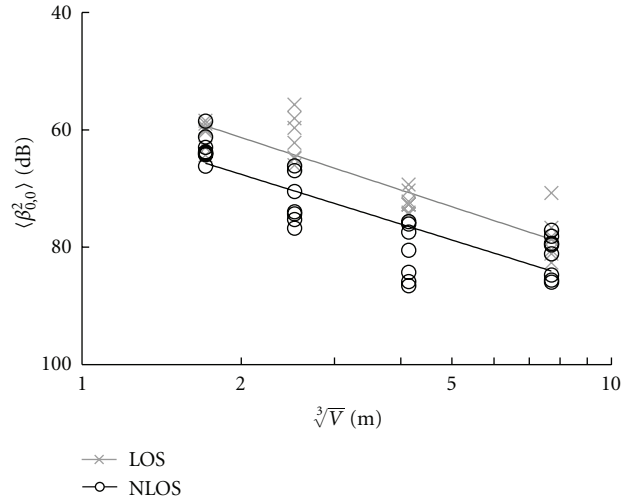

Figure 7: UWB propagation loss of the first ray within the first cluster against $V^{1/3}$.

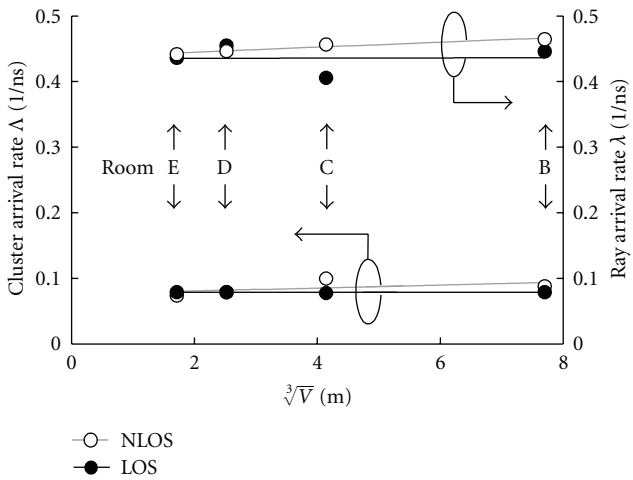

Figure 8: Arrival rates of clusters and rays within clusters.

Table 3: The parameter of decay factor functions for the cluster and the ray within the cluster.

		NLOS	LOS
Cluster	Γ' [ns/m]	1.25	0.70
	Γ_0 [ns]	10.0	7.1
Ray	γ' [ns/m]	0.28	0.11
	γ_0 [ns]	2.4	3.0

the ray power-decay factor on $V^{1/3}$, depicted in Figure 9, is formulated by

$$\Gamma = \Gamma_0 + \Gamma' \cdot \sqrt[3]{V}, \qquad \gamma = \gamma_0 + \gamma' \cdot \sqrt[3]{V}, \tag{6}$$

where Γ_0 and γ_0 are values of Γ and γ when imaginarily $V = 0$, Γ' and γ' are the slope of the cluster and the ray within the cluster against $V^{1/3}$, respectively. The values of Γ_0, γ_0, Γ', and γ' are listed in Table 3. Although the effect of shadowing has not been considered in this paper, it can be included in (2) after the same method as adopted in [6].

4. Realization of Onbody UWB Channels Based on the Composite Model

A composite statistical UWB channel model between onbody antennas is formulated by summing the models described in Section 3. A realization is calculated upon providing input data—whether the path is either LOS or NLOS—d (the distance between the antennas along the perimeter of the body), and the room volume, as shown in Figure 10. Once a number of realizations of the channel responses are calculated randomly, they are then served to estimate transmission performances (e.g., average bit error rates) and/or system capacity of communication systems, detection and false alarm rates of radar systems, and so forth, by simulation.

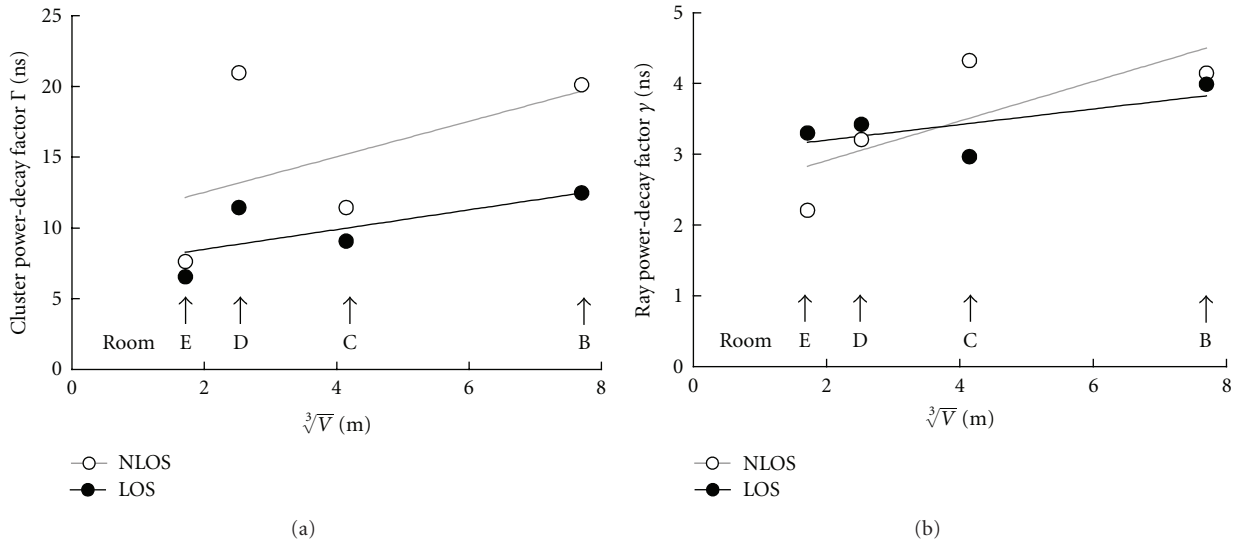

Figure 9: Power decay factors against $V^{1/3}$ for (a) the clusters and (b) the rays. The solid lines are the linear fitting.

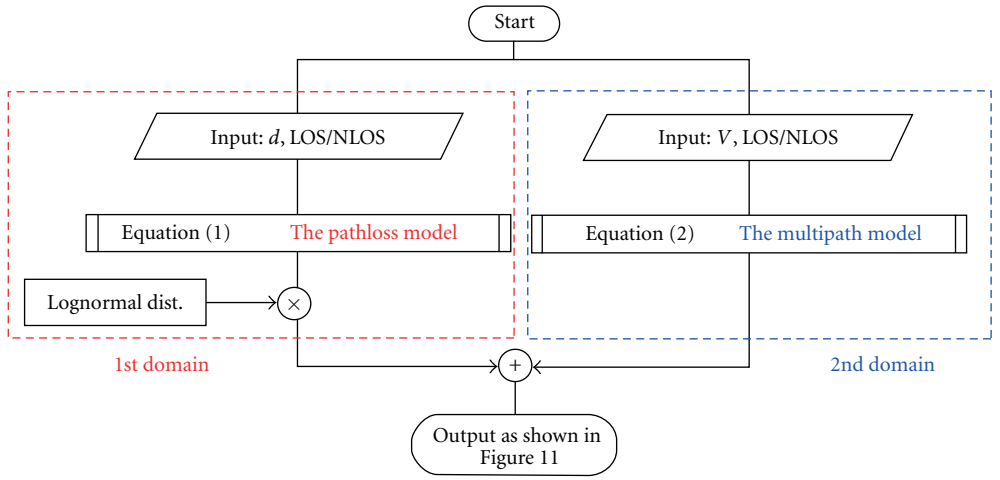

Figure 10: The flow chart of our model realization process.

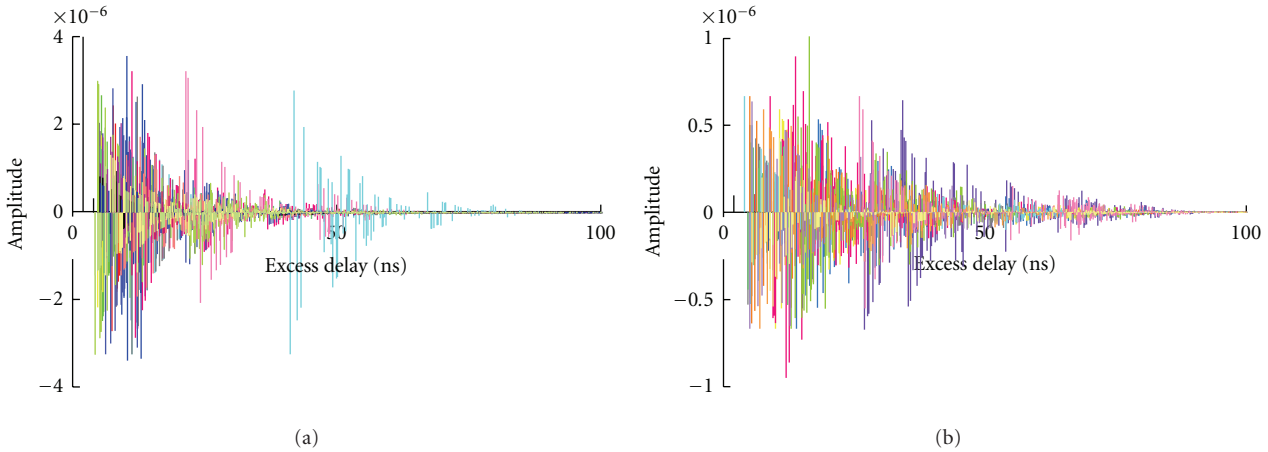

Figure 11: Examples of 20 channel response realizations for Room E ($V = 5\,\mathrm{m}^3$): (a) LOS and (b) NLOS.

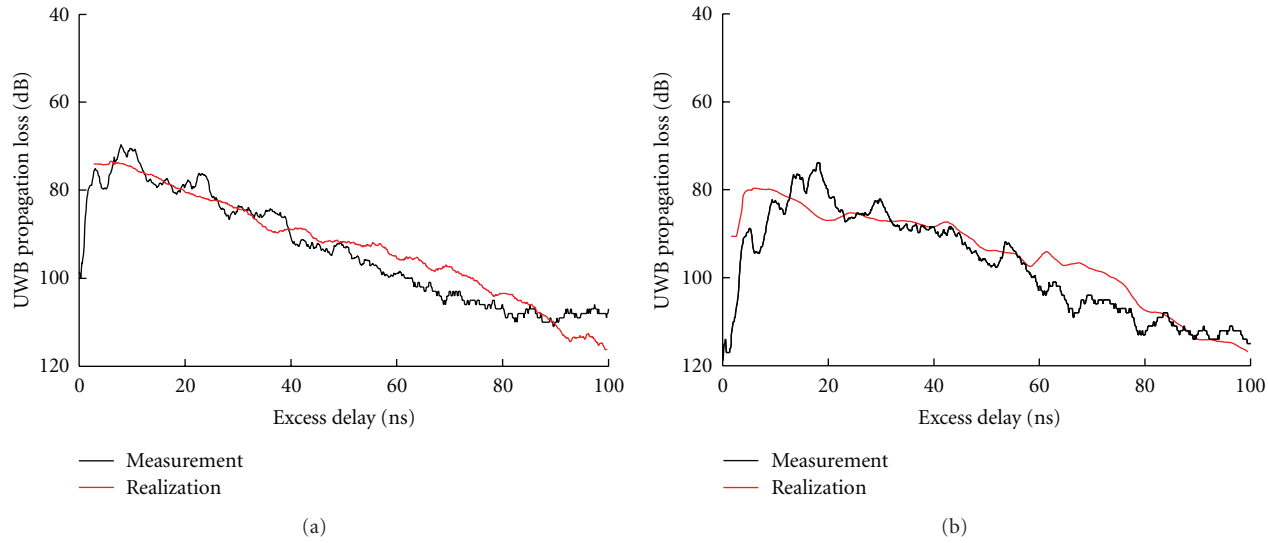

Figure 12: Comparison of the APDPs between 20 realizations and measured delay profiles of Room E ($V = 5\,\mathrm{m}^3$): (a) LOS and (b) NLOS.

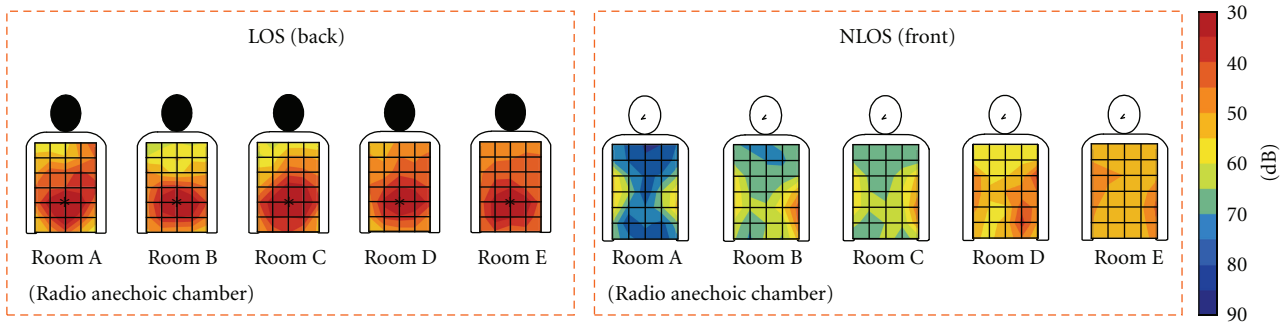

Figure 13: Spatial distribution of UWB propagation losses in the five rooms. The transmitting antenna was placed at point denoted by "*".

Examples of the channel response realizations for LOS and NLOS, assuming $d = 200\,\mathrm{mm}$ for LOS and 450 mm for NLOS and $V = 5\,\mathrm{m}^3$, are presented in Figure 11, where 20 realizations are overwritten. Average power delay profiles (APDPs) for LOS and NLOS were derived from these realizations and compared with the measured data. Moving average was conducted over a 3 ns period for calculating the APDPs. The APDPs derived from the calculated realizations and from the measured delay profiles reasonably agree, as shown in Figure 12. The validity of the proposed composite model was therefore confirmed.

5. Conclusions

In this study, a series of propagation measurements campaign were carried out between onbody antennas in five different rooms. A measured delay profile can be divided into two domains. In the first domain ($0 < t \leq 4\,\mathrm{ns}$), there is either a direct (for LOS) or diffracted (for NLOS) wave which depends on propagation distance along the perimeter of the body but essentially unrelated to room volume. This domain was modeled with a power decay law against the distance, and its amplitude followed a lognormal distribution. In the second domain ($t > 4\,\mathrm{ns}$), multipath components are dominant and dependent on room volume. Observations of the second domain indicate that rays generally arrive in clusters. Arrivals of clusters and rays within each cluster were found to be modeled by Poisson processes. As a result, the second domain was modeled by a modified Saleh-Valenzuela model with the use of lognormal distribution rather than Rayleigh distribution for multipath gain coefficients. Finally, the composite model to calculate the UWB onbody channel realizations was obtained by combining the two domains and validated with the use of the measured delay profiles.

Appendices

A. UWB Propagation Loss

Examples of spatial distributions of UWB propagation losses, measured in the same five rooms as those described in Section 2, are shown in Figure 13. The UWB propagation losses were calculated by integrating the power of the losses

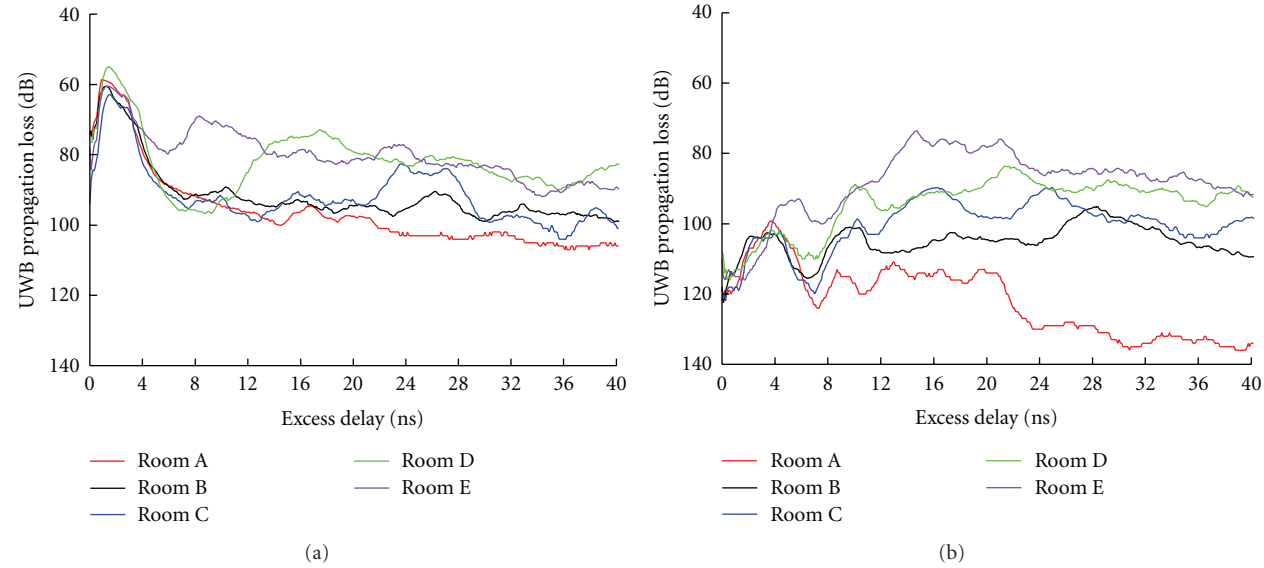

Figure 14: Measured average power delay profiles (averaged over 3 ns): (a) LOS and (b) NLOS.

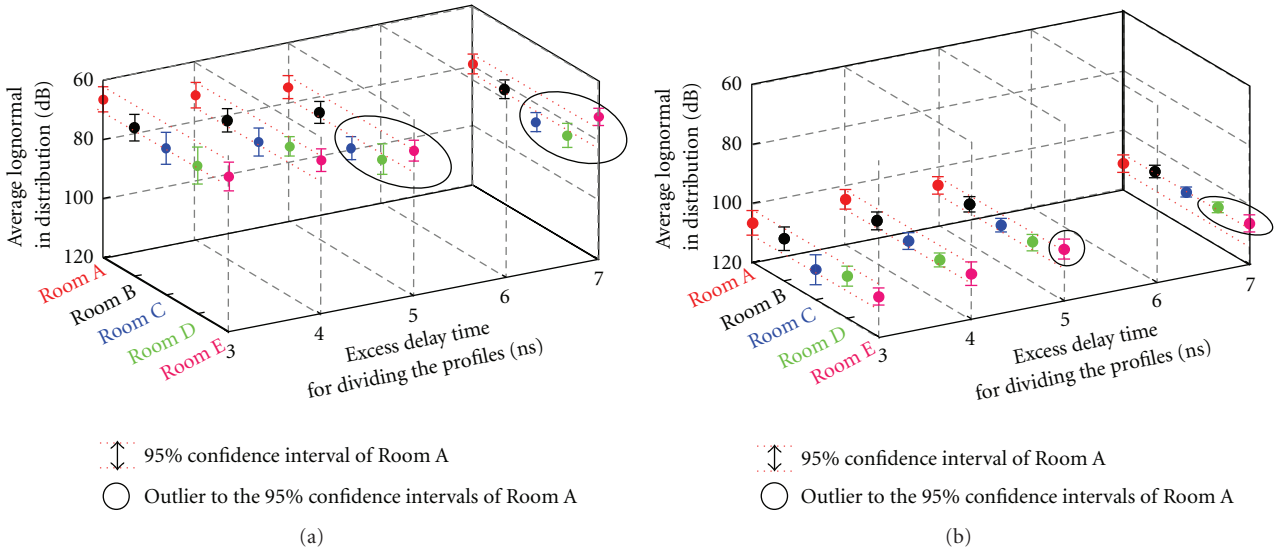

Figure 15: Averages in lognormal distribution fit to the propagation loss for Rooms A to E: (a) LOS and (b) NLOS. The dashed lines are the 95% confidence intervals of Room A (a radio anechoic chamber). The averages encircled by ovals are outliers to the 95% intervals of Room A.

between the feeding points of the antennas over occupied bandwidth:

$$\mathrm{PL_{dB}} = 10\log\left(\frac{1}{f_H - f_L}\int_{f_L}^{f_H} 10^{\mathrm{PL_{dB}}(f)/10}\,df\right), \qquad (A.1)$$

where $\mathrm{PL_{dB}}(f)$ is the propagation loss in dB measured at frequency f, and f_L and f_H are the lowest and highest frequencies. The propagation losses increased with decreasing the room volume, as shown in Figure 13.

B. Validity of 4 ns for Dividing the Delay Profiles

Figure 14 depicts average power delay profiles (averaged over 3 ns) for LOS and NLOS measured in Rooms A to E.

Curves are almost equal for a period between 0 and approximately 4 ns: the effect of the surrounding environment was insignificant up to 4 ns. Beyond the 4 ns, the propagation loss decreased (the curves move upward) with decreasing room volume. Furthermore, the amplitude distribution was examined to confirm the validity of t = 4 ns for dividing the delay profiles. The amplitudes within

the measured delay profiles were found to follow lognormal distribution up to an excess delay of 10 ns. The averages in the lognormal distribution up to 3, 4, 5, and 7 ns were estimated for LOS and NLOS, as shown in Figure 15, where the 95% confidence intervals derived of Room A data are plotted by dashed lines. While all the averages up to 4 ns for Rooms B to E fell within the 95% intervals, some (Rooms C, D, and E for LOS and Rooms D and E for NLOS) were outside the intervals, as shown in Figure 15. This fact also ratified the validity of $t = 4$ ns for dividing the profiles.

C. Proposed UWB Propagation Loss Model

Based on a series of propagation measurements conducted in a frequency bandwidth from 3.1 to 10.6 GHz, the authors proposed a UWB propagation loss model [5]:

$$\mathrm{PL_{dB}} = \mathrm{PL_{0dB}} + 10\left(n_\infty + \frac{n'}{\sqrt[3]{V}}\right)\log\left(\frac{d}{d_0}\right)[\mathrm{dB}], \qquad (C.1)$$

where $\mathrm{PL_{0dB}}$ is the propagation loss at the reference distance d_0 ($= 0.1$ m), n_∞ is the propagation loss exponent when the room volume $V = \infty$, and n' is the slope of n against $V^{-1/3}$. The values of $\mathrm{PL_{0dB}}$, n_∞, and n' for LOS and NLOS are given in [5].

Acknowledgments

This study was in part supported by the Japan Society for the Promotion of Science and the Academy of Finland with the Japan-Finland Bilateral Core Program. The authors would like to thank the program participants of the Tokyo Institute of Technology, Japan and Aalto University, Finland, for valuable discussions.

References

[1] T. Zasowski, F. Althaus, M. Stager, A. Wittneben, and G. Troster, "UWB for noninvasive wireless body area networks: channel measurements and results," in *Proceedings of the IEEE Conference on Ultrawideband Systems Technology (UWBST '03)*, pp. 285–289, November 2003.

[2] P. S. Hall and Y. Hao, Eds., *Antennas and Propagation for Body-Centric Wireless Communications*, Artech House, Boston, Mass, USA, 2006.

[3] A. Fort, J. Ryckaert, C. Desset, P. De Doncker, P. Wambacq, and L. Van Biesen, "Ultra-wideband channel model for communication around the human body," *IEEE Journal on Selected Areas in Communications*, vol. 24, no. 4, pp. 927–933, 2006.

[4] A. Sani, A. Alomainy, G. Palikaras et al., "Experimental characterization of UWB on-body radio channel in indoor environment considering different antennas," *IEEE Transactions on Antennas and Propagation*, vol. 58, no. 1, pp. 238–241, 2010.

[5] H. Yamamoto, M. Koiwai, and T. Kobayashi, "Measurements and modeling of ultra-wideband propagation losses around the human body dependent on room volume," *IEICE Transactions on Fundamentals of Electronics, Communications and Computer Sciences*, vol. E93, no. 12, pp. 2624–2633, 2010.

[6] A. F. Molisch, K. Balakrishnan, D. Cassioli et al., "IEEE 802. 15. 4a channel model—final report. Submitted to IEEE 802. 15 WPAN low rate alternative PHY task group 4a (TG4a)," Tech. Rep., IEEE 802. 15, 2004.

[7] C. Roblin, "On the separability of on-body and off-body clusters in the modeling of UWB WBAN channels for various indoor scenarios," in *Proceedings of the 5th European Conference on Antennas and Propagation (EUCAP '11)*, pp. 3148–3152, April 2011.

[8] Skycross, "3.1-10 GHz ultra-wideband antenna," http://www.Skycross.com/Products/PDFs/SMT-3TO10M-A.pdf.

[9] H. Yamamoto and T. Kobayashi, "Effects of feeding cable configurations on propagation measurements between small ultra wideband antennas for WBAN applications," in *Proceedings of the International Workshop on Future Wellness and Medical ICT Systems (FEELIT '08)*, September 2008.

[10] A. A. M. Saleh and R. A. Valenzuela, "A statistical model for indoor multipath propagation," *IEEE Journal on Selected Areas in Communications*, vol. 5, no. 2, pp. 128–137, 1987.

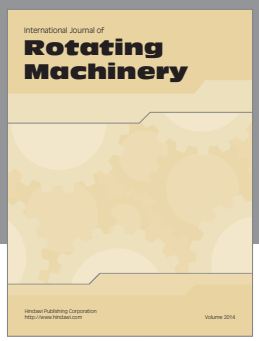

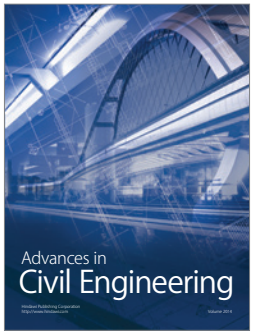

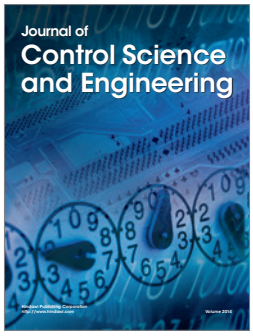

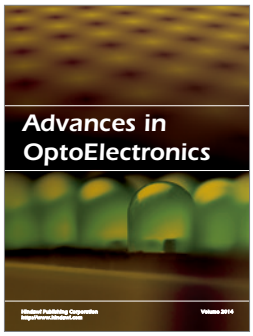

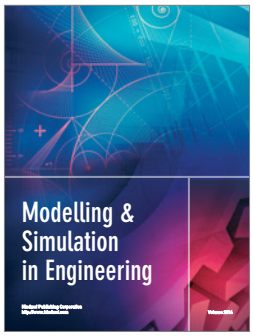

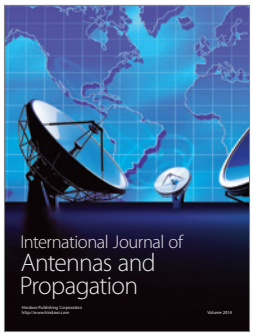

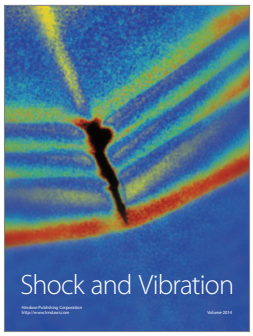

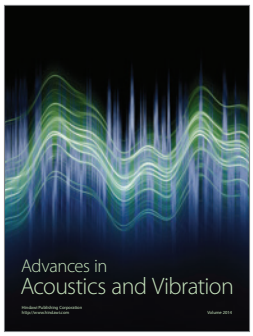

Hindawi

Submit your manuscripts at
http://www.hindawi.com